Effect of electron reflection on magnetized plasma sheath in an oblique magnetic field

Ting-Ting Wang, J. X. Ma, and Zi-An Wei

Citation: Physics of Plasmas **22**, 093505 (2015); doi: 10.1063/1.4930208
View online: http://dx.doi.org/10.1063/1.4930208
View Table of Contents: http://scitation.aip.org/content/aip/journal/pop/22/9?ver=pdfcov
Published by the AIP Publishing

Effect of electron reflection on magnetized plasma sheath in an oblique magnetic field

Ting-Ting Wang, J. X. Ma,[a] and Zi-An Wei
Department of Modern Physics and CAS Key Laboratory of Geospace Environment, University of Science and Technology of China, Hefei, Anhui 230026, People's Republic of China

(Received 15 May 2015; accepted 20 August 2015; published online 11 September 2015)

Magnetized plasma sheaths in an oblique magnetic field were extensively investigated by conventionally assuming Boltzmann relation for electron density. This article presents the study of the magnetized sheath without using the Boltzmann relation but by considering the electron reflection along the magnetic field lines caused by the negative sheath potential. A generalized Bohm criterion is analytically derived, and sheath profiles are numerically obtained, which are compared with the results of the conventional model. The results show that the ion Mach number at the sheath edge normal to the wall has a strong dependence on the wall potential, which differs significantly from the conventional model in which the Mach number is independent of the wall potential. The floating wall potential is lower in the present model than that in the conventional model. Furthermore, the sheath profiles are appreciably narrower in the present model when the wall bias is low, but approach the result of the conventional model when the wall bias is high. The sheath thickness decreases with the increase of ion-to-electron temperature ratio and magnetic field strength but has a complex relationship with the angle of the magnetic field. © *2015 AIP Publishing LLC*.
[http://dx.doi.org/10.1063/1.4930208]

I. INTRODUCTION

The topic of magnetized plasma-wall transition has been extensively studied in recent years because of its importance to magnetic fusion devices[1] and low-temperature plasma applications.[2,3] The plasma boundary region in an oblique magnetic field can usually be divided into three regions with different scalelengths, i.e., collisional presheath scaled with ion collision mean-free-path, magnetic presheath scaled with ion gyroradius evaluated with ion-sound speed, and non-neutral sheath scaled with Debye length.[4] Chodura studied the region of collisionless magnetic presheath[5] and showed that the ions enter the edge of the magnetic presheath along the magnetic field line with a velocity faster than or at least equal to the ion-acoustic speed. After that many others investigated the magnetic presheath using hydrodynamic model with ion collisions and discussed the effect of the magnetic field strength and orientation on the magnetic presheath.[6–9]

Recently, a number of researchers investigated the magnetized Debye sheath in which the magnetic field is sufficiently strong such that the ion gyro radius is comparable to the Debye length.[10–26] The magnetic field strength and orientation have a significant influence on the sheath structure and the Bohm criterion. In a collisionless magnetized sheath with cold ions, it was shown that the ion velocity normal to the wall at the sheath edge should be equal to the ion-acoustic speed,[12,13] i.e., the ion Mach number $M = 1$. In a hot magnetized plasma with finite ion temperature and accounting for the $\mathbf{E} \times \mathbf{B}$ drift velocity at the sheath boundary, Liu *et al.*[19] derived the critical ion Mach number (sheath criterion) $M^2 = T_i/T_e + \cos^2\theta$, where T_e and T_i are the electron and ion temperature and θ is the angle between the magnetic field and wall normal. The effects of the ionization and ion-neutral collisions lead to the decrease of M as well as the dependence of M on boundary electric field.[21,25] It was further shown that there exist both upper and lower limits of the Bohm velocity,[22,24] only within which the monotonic decrease of the ion density in the sheath occurs. Furthermore, the magnetized sheath structures in dusty[15–18] and electronegative plasmas[23–25] were investigated recently and it was shown that the presence of the charged dust strongly modifies the sheath structures, causing, for instance, the stratification of the dust density and potential profile.[16–18]

In the study of the magnetized plasma sheath, the electron density was conventionally assumed to obey the Boltzmann relation and the ions were modelled by fluid equations. Recently, a few authors investigated the magnetized sheath with the magnetic field strictly parallel to the wall, in which the Boltzmann relation is no longer hold for the electrons. They used the fluid equations for both the ions and electrons instead.[27–30]

In the magnetized sheath with the magnetic field oblique to the wall, the electrons, as they travel along the magnetic field line to the wall, will be partially reflected by the negative sheath potential. Thus, the Boltzmann relation no longer correctly describes the electron density distribution. In unmagnetized plasma sheaths, the electron reflection was studied and shown having a significant effect on the sheath structure, for example, causing the decrease of the wall potential.[31,32] In a magnetized sheath, Tskhakaya *et al.* considered the effect of the reflection of energetic and thermal electrons to study the potential drop and energy flux to the wall, and showed that a small population of the energetic electrons can significantly influence the potential drop and

[a]Author to whom correspondence should be addressed. Electronic mail: jxma@ustc.edu.cn

the energy flux to the wall.[10] However, the effects of the electron reflection on the magnetized sheath, especially on the generalized Bohm criterion and sheath profiles, have not been studied.

In this article, the magnetized plasma sheath in an oblique magnetic field is studied by taking the electron reflection into consideration. The ions are modelled by hot fluid equations. Section II presents the model, the derivation of the generalized Bohm criterion, and the floating wall potential. Section III gives the numerical results of the sheath profiles and their dependence on wall potential, magnetic field, and ion-to-electron temperature ratio. The detailed comparison of the present results with that of the Boltzmannian electrons is given. Section IV summarizes the main conclusions.

II. ANALYTIC MODEL

Consider a one-dimensional collisionless magnetized sheath shown in Fig. 1. Assume that the wall is parallel to $x-y$ plane and z axis is normal to the wall. Assume that the magnetic field $\mathbf{B}$ lies in $x-z$ plane with an angle θ to the z axis, i.e., $\mathbf{B} = B(\sin\theta\mathbf{e}_x + \cos\theta\mathbf{e}_z)$, where B is the magnitude of the magnetic field, and $\mathbf{e}_x$ and $\mathbf{e}_z$ are the unit vectors of the x and z direction. The y axis is in the direction of $\mathbf{E}\times\mathbf{B}$, with $\mathbf{E}$ being the sheath electric field along the z axis. For the one-dimensional sheath, the spatial variation is along the z axis, i.e., $\nabla = \mathbf{e}_z\partial/\partial z$. However, the ion velocity is three dimensional $\mathbf{v}_i = v_{ix}\mathbf{e}_x + v_{iy}\mathbf{e}_y + v_{iz}\mathbf{e}_z$, with v_{ix}, v_{iy}, and v_{iz} being the components in the rectangular coordinates. The x–y plane at $z=0$ is taken to be the presheath-sheath edge where the potential ϕ is assumed to be zero. The bulk plasma is somewhere in the $z<0$ region, so that the potential should be monotonically decreasing in the $z>0$ region.

In the magnetized sheath, the ion gyroradius is comparable to the Debye length which is much longer than the electron gyroradius. Thus, the electrons are frozen to the magnetic field lines. As the electrons travel along the field lines to the wall, some low velocity electrons will be reflected by the negative sheath potential before they reach the wall. Thus, the electrons consist of a forward-going (toward the wall) group and a reflected (backward-moving) group. Assume that the wall is perfect absorbing, i.e., the electrons reaching the wall will be totally absorbed, then, the velocity distribution function $f_e(z_w, v)$ at the wall surface

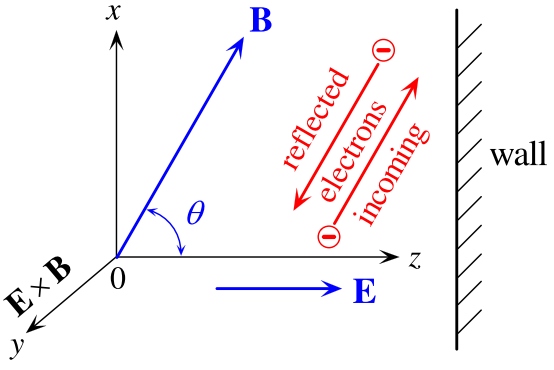

FIG. 1. Geometry of the magnetized sheath.

$z=z_w$ has a half Maxwellian form with velocity v extending from $v=0$ to $v=\infty$. Because of the reflection, the distribution function $f_e(z,v)$ at an arbitrary position z in front of the wall will have a truncated Maxwellian form including the forward-going ($v=0$ to ∞) and backward-moving ($v=-v_m$ to 0) electrons. Thus, the electron density n_e at z is given by

$$n_e = \int_{-v_m}^{\infty} f_e(z,v)dv, \tag{1}$$

where the maximum velocity of the backward-moving electrons, v_m, is determined by those electrons reflected infinitesimally close to the wall surface and moving back to the point z. By energy conservation, v_m is given by

$$v_m = \sqrt{\frac{2e[\phi(z)-\phi_w]}{m_e}}, \tag{2}$$

where $-e$ and m_e are the electron charge and mass, $\phi(z)$ and ϕ_w are the potential at z and z_w, respectively. Assume that at $z=0$ the forward-going electrons have a half Maxwellian distribution $f_e^+(0, v_0 \geq 0) = A\exp(-m_e v_0^2/2T_e)$, where T_e is electron temperature and A is a normalization constant. The reflected electrons have the same distribution except that the velocity direction is reversed. Because of the conservations of the energy and flux, the distribution function at the point z is

$$f_e(z,v) = A\exp\left(-\frac{\frac{1}{2}m_e v^2 - e\phi(z)}{T_e}\right) \tag{3}$$

for $-v_m \leq v < \infty$. Substituting it into Eq. (1), we obtain

$$n_e = A\frac{\sqrt{\pi}}{2}v_{te}\exp\left(\frac{e\phi}{T_e}\right)\left[1+\mathrm{erf}\left(\frac{v_m}{v_{te}}\right)\right], \tag{4}$$

where $v_{te} = (2T_e/m_e)^{1/2}$ is the electron thermal velocity and $\mathrm{erf}(x) = 2\pi^{-1/2}\int_0^x \exp(-t^2)dt$ is the error function. In Eq. (4), the first term on the right-hand-side represents the density of the forward-going electrons since it is resulted from the integration of Eq. (1) from 0 to ∞, while the second term containing the error function is the density of reflected electrons.

At the presheath-sheath edge, the quasi-neutrality condition $n_{e0} = n_{i0} = n_0$ must be satisfied, where n_0 is the density of the quasi-neutral plasma at the sheath edge, and hereafter, the subscript "0" represents the quantities at $z=0$. Thus, the normalization constant A can be determined

$$\frac{\sqrt{\pi}}{2}v_{te}A = \frac{n_0}{1+\mathrm{erf}\left(\sqrt{-e\phi_w/T_e}\right)} = n_{e0}^+ \tag{5}$$

with n_{e0}^+ representing the density of the forward-going electrons at $z=0$. Using Eqs. (2) and (5), the electron density can be rewritten as

$$n_e = n_{e0}^+\exp\left(\frac{e\phi}{T_e}\right)\left[1+\mathrm{erf}\left(\sqrt{\frac{e(\phi-\phi_w)}{T_e}}\right)\right]. \tag{6}$$

The ions are described by collisionless hot fluid equations

$$\frac{\partial}{\partial z}(n_i v_{iz}) = 0, \tag{7}$$

$$m_i n_i v_{iz}\frac{\partial \mathbf{v}_i}{\partial z} = e n_i\left(-\frac{\partial \phi}{\partial z}\mathbf{e}_z + \mathbf{v}_i \times \mathbf{B}\right) - T_i\frac{\partial n_i}{\partial z}\mathbf{e}_z, \tag{8}$$

where n_i, m_i, and T_i are the density, mass, and temperature of the ions, respectively. The system is closed by Poisson equation

$$\partial^2\phi/\partial z^2 = e(n_e - n_i)/\epsilon_0, \tag{9}$$

where ϵ_0 is the vacuum dielectric constant.

It is convenient to define the dimensionless quantities

$$N_{e,i} = \frac{n_{e,i}}{n_0}, \quad \Phi = \frac{e\phi}{T_e}, \quad \mathbf{u} = \frac{\mathbf{v}_i}{c_s},$$
$$\xi = \frac{z}{\lambda_D}, \quad T = \frac{T_i}{T_e}, \quad \Omega = \frac{\omega_{ci}}{\omega_{pi}},$$

where $c_s = (T_e/m_i)^{1/2}$ is the ion sound velocity, $\lambda_D = (\epsilon_0 T_e/e^2 n_0)^{1/2}$ is the Debye length, $\omega_{ci} = eB_0/m_i$ is ion gyrofrequency, and $\omega_{pi} = c_s/\lambda_D$ is ion plasma frequency. Using these quantities, Eqs. (5)–(9) can be simplified

$$N_{e0}^{+} = \frac{n_{e0}^{+}}{n_0} = \frac{1}{1+\mathrm{erf}\left(\sqrt{-\Phi_w}\right)}, \tag{10}$$

$$N_e = N_{e0}^{+}\exp(\Phi)[1+\mathrm{erf}(\sqrt{\Phi-\Phi_w})], \tag{11}$$

$$N_i = N_{i0}u_{z0}/u_z = u_{z0}/u_z, \tag{12}$$

$$u_z\frac{du_x}{d\xi} = \Omega u_y\cos\theta, \tag{13}$$

$$u_z\frac{du_y}{d\xi} = \Omega u_z\sin\theta - \Omega u_x\cos\theta, \tag{14}$$

$$u_z\frac{du_z}{d\xi} = \frac{u_z^2}{u_z^2 - T}\left(-\frac{d\Phi}{d\xi} - \Omega u_y\sin\theta\right), \tag{15}$$

$$\frac{d^2\Phi}{d\xi^2} = N_e - N_i. \tag{16}$$

Here, u_x, u_y, u_z denote the components of $\mathbf{u}$ in the coordinates, and Eq. (12) has been used in obtaining Eq. (15).

Comparing with the conventional model of applying the Boltzmann relation to the electron density, i.e., $N_{e\mathrm{B}} = \exp(\Phi)$, the electron density in the present model is lower by a factor of

$$\frac{N_e}{N_{e\mathrm{B}}} = \frac{1+\mathrm{erf}\left(\sqrt{\Phi-\Phi_w}\right)}{1+\mathrm{erf}\left(\sqrt{-\Phi_w}\right)}, \tag{17}$$

which depends on the wall potential Φ_w. For sufficiently large negative wall potential, the electron density tends to be equal to that of the Boltzmannian model.

A. Generalized Bohm criterion

In order to form a stationary ion sheath with monotonically decreasing potential, the ion density must be higher than the electron density in the whole sheath region. This requires that the decrease of the ion density should be slower than that of the electron density near the sheath edge since at the sheath edge the electron and ion density are equal, i.e.,

$$\frac{\partial N_i}{\partial \xi} \geq \frac{\partial N_e}{\partial \xi}. \tag{18}$$

Using Eqs. (11), (12), (15), and the boundary conditions $\Phi = 0$ and $N_{i0} = N_{e0} = 1$ at $\xi = 0$, we obtain the generalized Bohm criterion for the $z-$component of the ion velocity at the sheath edge

$$u_{z0}^2 \geq T + \frac{1 - \Omega u_{y0}\sin\theta/\mathcal{E}_0}{1 + N_{e0}^{+}\exp(\Phi_w)/\sqrt{-\pi\Phi_w}}, \tag{19}$$

where $\mathcal{E}_0 = -d\Phi/d\xi$ is the dimensionless electric field at the sheath edge. Eq. (19) shows that u_{z0} is related to the y-component of the ion boundary velocity u_{y0}. To determine the boundary values u_{x0} and u_{y0}, we recall that in the magnetic presheath whose scalelength is much longer than the ion gyroradius, the ions, being accelerated by the weak presheath electric field, stream along the magnetic field lines and in the meantime their gyrocenters drift perpendicularly to the magnetic field because of the $\mathbf{E}\times\mathbf{B}$ and diamagnetic drifts which are in the y direction. Thus, at the presheath-sheath edge, u_y can be taken as the $\mathbf{E}\times\mathbf{B}$ drift velocity (diamagnetic drift can be neglected if $T_e \gg T_i$), i.e., $u_{y0} = \mathcal{E}_0\sin\theta/\Omega$,[19] while $u_{x0} = u_{||}\sin\theta = u_{z0}\tan\theta$.[25] Substituting u_{y0} into Eq. (19) yields

$$u_{z0} \geq M_c = (T + C\cos^2\theta)^{1/2}, \tag{20}$$

where the coefficient $C < 1$ depends on the wall potential

$$C = \frac{\sqrt{-\pi\Phi_w}}{\sqrt{-\pi\Phi_w} + N_{e0}^{+}\exp(\Phi_w)}. \tag{21}$$

It is shown that the critical Mach number M_c is independent of the boundary electric field. However, M_c is a function of the wall potential Φ_w, which differs significantly from the model using the Boltzmann relation for the electron density. In the limit $\Phi_w \to -\infty$,

$$M_c \to (T + \cos^2\theta)^{1/2} = M_{cB}, \tag{22}$$

which is the result of the Boltzmannian-electron model.[19,25] Fig. 2 clearly reveals this difference by showing the variation of M_c with respect to the wall potential for the two models. For the present model, M_c decreases with the increase of the wall potential, while for the Boltzmannian-electron model, it is a constant. M_c deviates substantially from the value of the Boltzmannian-electron model if the wall bias $|\Phi_w|$ is low. However, the deviation nearly vanishes when $|\Phi_w| \geq 4$.

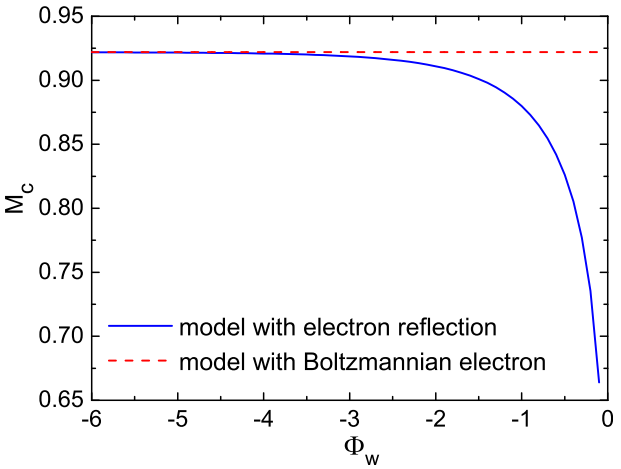

FIG. 2. Critical ion Mach number M_c versus wall potential Φ_w for the case $T_i/T_e = 0.1$ and $\theta = 30°$. Solid line: the model with electron reflection. Dashed line: the model using Boltzmann relation.

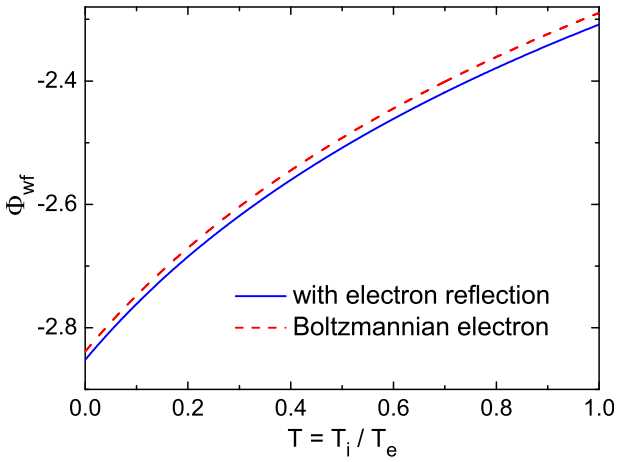

FIG. 3. Floating wall potential Φ_{wf} versus ion-to-electron temperature ratio $T = T_i/T_e$ for $m_i/m_e = 1836$ and $\theta = 45°$. Solid line: the model with electron reflection. Dashed line: the model using Boltzmann relation.

B. Floating wall potential

The floating wall potential is determined by the balance of the electron and ion fluxes to the wall, i.e., $\Gamma_{ew}\cos\theta = \Gamma_{iw}$, where Γ_{ew} is the electron flux along the magnetic field line (which is not affected by the magnetic field) and Γ_{iw} is the ion flux normal to the wall. From the continuity equation (7), the ion flux is a constant

$$\Gamma_{iw} = n_0 u_{z0} c_s. \tag{23}$$

Since at the wall surface there are no reflected electrons, the electron flux is obtained from Eqs. (3) and (5)

$$\Gamma_{ew} = \int_0^\infty v f(z_w, v) dv = \frac{1}{\sqrt{\pi}} v_{te} n_{e0}^{+} \exp(\Phi_w). \tag{24}$$

Using Eq. (20) for u_{z0}, we obtain the equation for the floating wall potential Φ_{wf}

$$M_c \exp(-\Phi_{wf})\left[1 + \mathrm{erf}\left(\sqrt{-\Phi_{wf}}\right)\right] = \sqrt{\frac{2m_i}{\pi m_e}}\cos\theta. \tag{25}$$

By comparison, in the model of using the Boltzmann relation, the electron flux at the wall is[2]

$$\Gamma_{ewB} = \frac{1}{2\sqrt{\pi}} v_{te} n_0 \exp(\Phi_{wB}) \tag{26}$$

which yields the floating wall potential

$$\Phi_{wfB} = \ln\left(\sqrt{\frac{2\pi m_e}{m_i}\left(1 + \frac{T}{\cos^2\theta}\right)}\right). \tag{27}$$

Figures 3 and 4 present the comparison of the floating wall potential versus the ion-to-electron temperature ratio T and the magnetic field incident angle θ between the two models. For both models, the floating wall potential increases with T and θ. However, Φ_{wf} is lower (the magnitude is higher) for the model with the electron reflection than that for the model with the Boltzmannian electrons. This difference can be manifested by the fact that the electron wall-flux is higher in the former than in the latter model, which can be seen by comparing Eqs. (24) and (26) with the help of Eq. (10). This requires a higher ion flux (Mach number) to balance the electron flux for the former model. Thus, from Fig. 2, the wall potential drops (its magnitude increases) in order to raise the ion Mach number.

The reason for the increase of Φ_{wf} with T is that the critical ion Mach number and hence the ion-wall flux increase with T, which in turn requires a weaker wall potential (smaller $|\Phi_{wf}|$) to reflect the incoming electrons in order to maintain the current balance. On the other hand, the electron flux normal to the wall is proportional to $\cos\theta$, which decreases with θ. For the same reason, a smaller $|\Phi_{wf}|$ is needed to maintain the current balance. Thus, Φ_{wf} increases with θ.

III. NUMERICAL RESULTS

For an arbitrarily biased wall potential, the set of equations (11)–(16) are numerically solved, using the boundary conditions formulated in Sec. II A. In addition, a weak

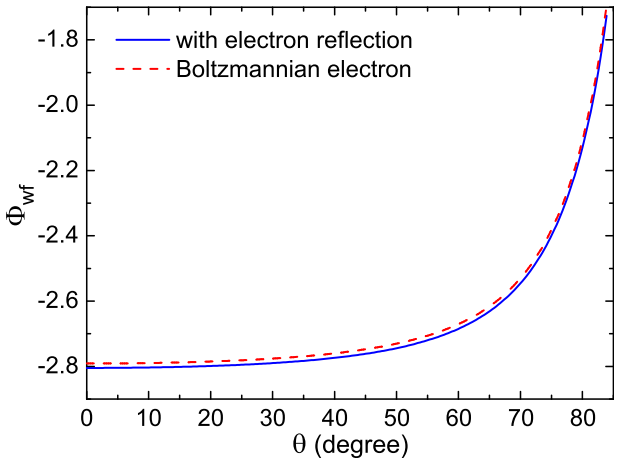

FIG. 4. Floating wall potential Φ_{wf} versus the incident angle of the magnetic field θ for $m_i/m_e = 1836$ and $T_i/T_e = 0.1$. Solid line: the model with electron reflection. Dashed line: the model using Boltzmann relation.

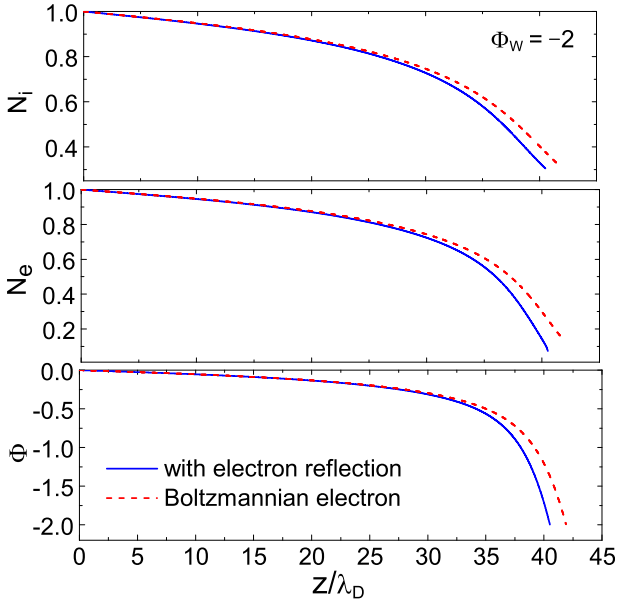

FIG. 5. The comparison of the distributions of the ion and electron densities and potential in the sheath between the two models for a low wall bias $\Phi_w = -2$. Other parameters are $T_i/T_e = 0.1$, $\theta = 60°$, and $\omega_{ci}/\omega_{pi} = 0.1$. Solid lines: the model with electron reflection. Dashed lines: the model using Boltzmann relation.

boundary electric field $\mathcal{E}_0 = 0.005$ is assumed in order to start the calculation. The results are presented in Figs. 5–9.

A. Effect of wall potential on sheath profiles

The comparisons of the distributions of the plasma densities and potential with respect to the distance between the two models are plotted in Figures 5 and 6 for different wall potentials. It is shown that, for a low wall potential $|\Phi_w| = 2$, the sheath profiles exhibit obvious differences between the two models. The sheath is thinner in the model with the electron reflection than in the Boltzmannian-electron model.

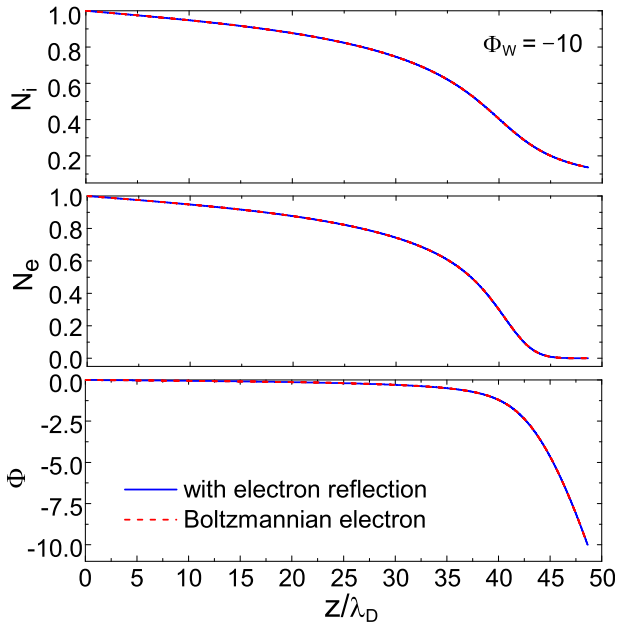

FIG. 6. Same as Fig. 5 except for a higher wall bias $\Phi_w = -10$.

However, the differences nearly disappear for a high wall potential $|\Phi_w| = 10$. This difference can be explained by Eq. (17). At the low wall potential, the electron density in the model with the reflection is appreciably lower than that in the Boltzmannian-electron model, which results in the quicker decrease of the electron density inside the sheath and hence the narrowing of the sheath. At the high wall potential, the difference in the electron density between the two models becomes small, and hence, the sheath profiles become indistinguishable.

B. Effect of ion temperature on sheath profiles

For a given wall potential, a magnetic field strength, and an incident angle, the effect of the ion temperature on the potential distributions is shown in Fig. 7. It is seen that, with the increase of the ion temperature, the sheath profiles shrink and the difference between the two models slightly reduces. This can be mainly attributed to the effect of the ion boundary velocity component u_{z0} along the z direction. Since u_{z0} increases with T as can be seen from Eq. (20), the relative increase in u_z (i.e., u_z/u_{z0}) inside the sheath is slower in the high T case than that in the low T case. By the flux conservation Eq. (12), $N_i = u_{z0}/u_z$ is higher in the high T case. Thus, the net space charge $N_i - N_e$ and subsequently the sheath electric field are higher in the high T case, which results in the narrowing of the sheath.

We note that the electron densities, N_e and N_{eB}, for the two models are independent of T. The ion fluid equations, Eqs. (12)–(15), on the other hand, are independent of the two models. However, the ion boundary velocity u_{z0} does differ between the two models, as can be seen from Eqs. (20) and (22). With the increase of T, N_e and N_{eB} do not change, but the difference in M_c and M_{cB} becomes smaller. Accordingly, the difference between the ion densities for the two models becomes smaller. Therefore, the difference in the sheath profiles between the two models slightly decreases in the high T case.

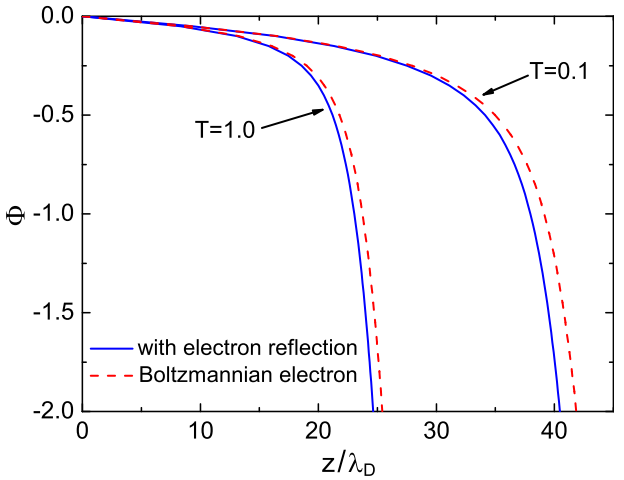

FIG. 7. The potential distributions in the sheath for two ion temperatures $T_i/T_e = 0.1$ and 1.0. Other parameters are $\theta = 60°$, $\omega_{ci}/\omega_{pi} = 0.1$, and $\Phi_w = -2$. Solid lines: the model with electron reflection. Dashed lines: the model using Boltzmann relation.

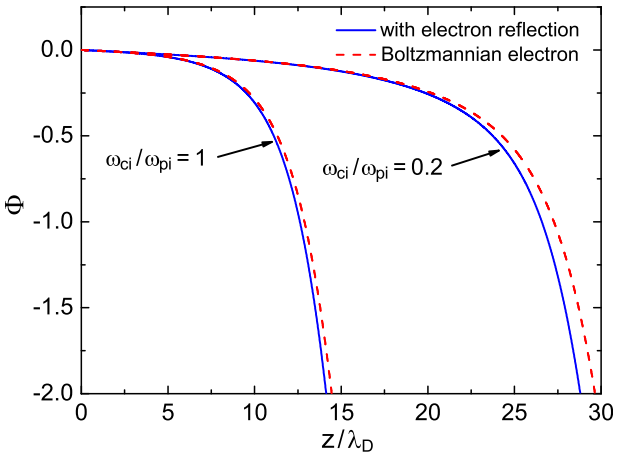

FIG. 8. The potential distributions in the sheath for two values of $\omega_{ci}/\omega_{pi} = 0.2$ and 1. Other parameters are $\theta = 60^\circ$, $T_i/T_e = 0.1$, and $\Phi_w = -2$. Solid lines: the model with electron reflection. Dashed lines: the model using Boltzmann relation.

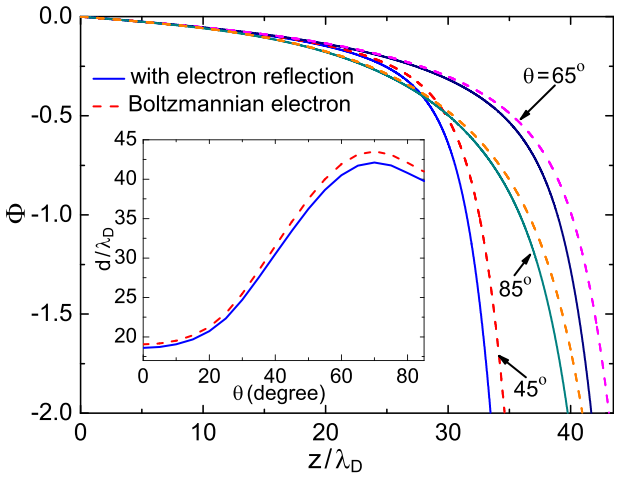

FIG. 9. The variation of the potential profile with the incident angle θ of the magnetic field. The inset shows the sheath thickness d/λ_D versus θ. The parameters are $T_i/T_e = 0.1$, $\omega_{ci}/\omega_{pi} = 0.1$, and $\Phi_w = -2$. Solid lines: the model with electron reflection. Dashed lines: the model using Boltzmann relation.

C. Effect of magnetic field on sheath profiles

Figure 8 shows the influence of the magnetic field strength on the potential profiles. When the wall potential, the ion temperature, and the incident angle of the magnetic field are fixed, the stronger the magnetic field strength is, the narrower the sheath will be. Furthermore, the difference between the two models becomes smaller. The strong magnetic field enhances the ion gyro motion, which hinders the ion acceleration by the sheath electric field. Thus, the increase of the ion velocity component u_z along the z direction is delayed. By the flux conservation, the decrease of the ion density towards the wall slows down. However, the electron density drop remains unchanged for the same potential drop. Therefore, the net space charge increases, which in turn results in the increase of the electric field and hence the shortening of the sheath.

The dependence of the potential profiles on the incident angle of the magnetic field, plotted in Fig. 9, shows a complex behaviour. When the other parameters are fixed, the variation of the sheath thickness d (distance from the sheath edge to the wall) with respect to θ exhibits a maximum around $\theta \sim 70^\circ$, before which d increases with θ and after which d decreases with θ. Further, the difference between the sheath thicknesses for the two models enlarges with the increase of θ.

To explain this phenomenon, we note that the electron density is independent of the magnetic field. The ion density is given by $N_i = u_{i0}/u_i$. There are two effects of θ on N_i. The first is that u_{z0} (i.e., the critical Mach number, Eq. (20)) decreases with the increase of θ, which in turn causes the decrease of N_i and net space charge $N_i - N_e$. Thus, it tends to broaden the sheath profile. The second is that, from Eq. (15), the increase of θ results in the decrease of $du_z/d\xi$, which means that the increase of u_z toward the wall slows down. Thus, u_z is smaller, and N_i is higher in the larger θ case, which leads to the shrink of the sheath. For small θ, the second effect is weak because of its dependence on $\sin\theta$; thus, the first effect dominates the second, and therefore, the sheath thickness increases with θ. For large θ, on the other hand, the first effect is weak because of its dependence on $\cos\theta$; thus, the second effect dominates the first and the sheath thickness decreases with θ. The interplay of the two effects results in the complex dependence of the sheath thickness on θ shown in Fig. 9.

IV. CONCLUSION

The magnetized sheath with magnetic field oblique to the wall is studied for the model considering the effect of the electron reflection by the negative sheath potential. The generalized Bohm criterion is derived which shows that the critical ion Mach number depends sensitively on the wall potential Φ_w, which differs significantly from the conventional model in which the Mach number is independent of Φ_w. For the present model, it is shown that the floating wall potential is appreciably lower than that of the conventional model, and it increases with the ion-to-electron temperature ratio and the incident angle of the magnetic field. The numerical results reveal that the sheath profiles deviate from that of the conventional model at small $|\Phi_w|$, but the deviation vanishes at large $|\Phi_w|$. The sheath thickness decreases with the increase of the ion-to-electron temperature ratio and the magnetic field strength. In addition, the variation of the sheath thickness with respect to the incident angle of the magnetic field exhibits a maximum at certain angle.

ACKNOWLEDGMENTS

This work was supported by the National Natural Science Foundation of China (Grant Nos. 11175177 and J1103207).

[1]P. C. Stangeby, *The Plasma Boundary of Magnetic Fusion Devices* (IoP Publishing, Bristol and Philadelphia, 2000).
[2]M. A. Lieberman and A. J. Lichtenberg, *Principles of Plasma Discharges and Materials Processing* (John Wiley and Sons, Inc., New York, 1994).
[3]K. Ostrikov, E. C. Neyts, and M. Meyyappan, Adv. Phys. **62**, 113 (2013).
[4]E. Ahedo, Phys. Plasmas **4**, 4419 (1997).
[5]R. Chodura, Phys. Fluids **25**, 1628 (1982).
[6]K.-U. Riemann, Phys. Plasmas **1**, 552 (1994).

[7]P. C. Stangeby, Phys. Plasmas **2**, 702 (1995).
[8]I. I. Beilis and M. Keidar, Phys. Plasmas **5**, 1545 (1998).
[9]T. M. G. Zimmermann, M. Coppins, and J. E. Allen, Phys. Plasmas **15**, 072301 (2008).
[10]D. Tskhakaya, S. Kuhn, V. Petrzilka, and R. Khanal, Phys. Plasmas **9**, 2486 (2002).
[11]X. Zou, J.-Y. Liu, Y. Gong, Z.-X. Wang, Y. Liu, and X.-G. Wang, Vacuum **73**, 681 (2004).
[12]N. Sternberg and J. Poggie, IEEE Trans. Plasma Sci. **32**, 2217 (2004).
[13]R. N. Franklin, J. Phys. D: Appl. Phys. **38**, 3412 (2005).
[14]S. F. Masoudi, J. Phys. D: Appl. Phys. **40**, 6641 (2007).
[15]B. P. Pandey, A. Samarian, and S. V. Vladimirov, Plasma Phys. Controlled Fusion **50**, 055003 (2008).
[16]G. Foroutan, H. Mehdipour, and H. Zahed, Phys. Plasmas **16**, 103703 (2009).
[17]H. Mehdipour and G. Foroutan, Phys. Plasmas **17**, 083704 (2010).
[18]H. Mehdipour, I. Denysenko, and K. Ostrikov, Phys. Plasmas **17**, 123708 (2010).
[19]J. Liu, F. Wang, and J. Sun, Phys. Plasmas **18**, 013506 (2011).
[20]A. K. Shaw, S. Kar, K. S. Goswami, and B. J. Saikia, Phys. Plasmas **19**, 012120 (2012).
[21]J. Ou and J. Yang, Phys. Plasmas **19**, 113504 (2012).
[22]M. M. Hatami and B. Shokri, Phys. Plasmas **19**, 083510 (2012).
[23]A. K. Shaw, S. Kar, and K. S. Goswami, Phys. Plasmas **19**, 102108 (2012).
[24]M. M. Hatami and B. Shokri, Phys. Plasmas **20**, 033506 (2013).
[25]J.-J. Li, J. X. Ma, and Z. Wei, Phys. Plasmas **20**, 063503 (2013).
[26]D. D. Tskhakaya, Sr. and L. Kos, Phys. Plasmas **21**, 102115 (2014).
[27]D. D. Tskhakaya, P. K. Shukla, B. Eliasson, and S. Kuhn, Phys. Plasmas **12**, 103503 (2005).
[28]B. P. Pandey, A. Samarian, and S. V. Vladimirov, Phys. Plasmas **14**, 093703 (2007).
[29]T. M. G. Zimmermann, M. Coppins, and J. E. Allen, Phys. Plasmas **16**, 043501 (2009); **17**, 022301 (2010).
[30]N. S. Krasheninnikova, X. Tang, and V. S. Roytershteyn, Phys. Plasmas **17**, 057103 (2010).
[31]J. P. Sheehan *et al*., Phys. Rev. Lett. **111**, 075002 (2013).
[32]J. P. Sheehan, I. D. Kaganovich, H. Wang, D. Sydorenko, Y. Raitses, and N. Hershkowitz, Phys. Plasmas **21**, 063502 (2014).